

Breakdown electron-hole symmetry in graphene structure with a semiconductor gate

F. T. Vasko*

QK Applications, 3707 El Camino Real, San Francisco, CA 94033, USA

(Dated: October 6, 2018)

The electron-hole symmetry in the structure “graphene - insulating substrate -semiconductor gate” is violated due to an asymmetrical drop of potential in the semiconductor gate under positive or negative biases. The gate voltage dependencies of concentration and conductivity are calculated for the case of SiO₂ substrate placed over low- (moderate-) doped *p*-Si. Similar dependencies of the optical conductivity are analyzed for the case of high- κ substrates (AlN, Al₂O₃, HfO₂, and ZrO₂). The comparison of our results with experimental data shows a good agreement for both cases.

PACS numbers: 72.80.Vp, 73.40.Ty, 78.67.Wj

The energy spectrum and scattering mechanisms in graphene are symmetric with respect to electron-hole replacement, so that the transport phenomena are identical for the electron and hole doping cases, see reviews 1 and 2. According to the theoretical analysis, as well as the transport and optical measurements (see review [3] and references therein), the Coulomb renormalization in graphene leads to weak ($\sim 10\%$ for typical parameters) asymmetry of electron and hole responses. These results were obtained for the electrostatically doped graphene structures with metallic (or heavily-doped semiconductor) gates. The sheet concentration of carriers, n_g , is determined by the gate voltage V_g according to the plane capacitor formula

$$n_g = \alpha(V_g - V_0), \quad \alpha \approx \frac{\epsilon_s}{4\pi|e|d}, \quad (1)$$

where ϵ_s is the dielectric permittivity of substrate of thickness d , see Fig. 1a, and voltage V_0 corresponds to the electroneutrality point; below we suppose $V_0 \rightarrow 0$. Thus, transport phenomena should be symmetric with respect to the sign flip of V_g (electron-hole symmetry). But this symmetry appears to be violated for the structures with low- (moderate-) doped semiconductor gates. It is due to differences in the drop of potential and charge distributions for positive or negative biases, when the depleted or heavily-doped regions appear, see Figs. 1b and 1c, respectively. This simple mechanism was not analyzed yet and it is timely to re-examine Eq. (1) for the case of low-doped semiconductor gates, which were used in several experiments. [4–6]

In this letter we solve the electrostatic problem for graphene structures with thick SiO₂ or thin high- κ (AlN, Al₂O₃, HfO₂, and ZrO₂) substrates placed over *p*-Si of different doping levels. The gate voltage dependencies of the concentration and the dc conductivity as well as the interband optical conductivity are calculated and comparisons with the experimental data [4–6] are performed.

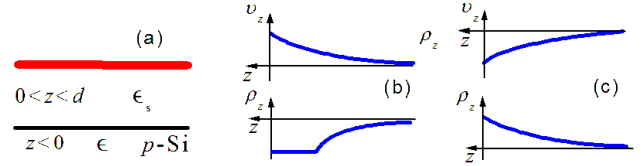


FIG. 1: (a) Structure schematic for back-gated graphene (grey) with dielectric substrate of thickness d and permittivity ϵ_s over *p*-doped Si of permittivity ϵ . (b) and (c) Potential (upper) and charge (lower) distributions along semiconductor gate for the electron and hole doped Si cases, respectively.

The distribution of the electrostatic potential φ_z across the structure under consideration (along z -axis, $z \leq d$) is governed by the Poisson equation

$$\frac{d}{dz} \left(\epsilon_z \frac{d\varphi_z}{dz} \right) = -4\pi\rho_z, \quad \epsilon_z = \begin{cases} \epsilon_s, & 0 < z < d \\ \epsilon, & z < 0 \end{cases}, \quad (2)$$

where ϵ_z stands for the dielectric permittivity and ρ_z is the charge density in graphene (at $z \rightarrow d$) and in Si gate (at $z < 0$). Using the Gauss theorem at $z \rightarrow d - 0$ and connecting the derivatives of φ_z at $z \rightarrow 0$ one obtains the boundary conditions

$$\left. \frac{d\varphi_z}{dz} \right|_{z=d-0} = \frac{4\pi}{\epsilon} \sigma_g, \quad \epsilon_z \left. \frac{d\varphi_z}{dz} \right|_{-0}^{+0} = 0. \quad (3)$$

Here $\sigma_g = \int_{d-0}^{d+0} dz \rho_z = \mp |e| n_g$ is the charge density induced in graphene which is written through n_g and $-$ or $+$ correspond to the electron or hole doping. The linear potential distribution $\varphi_z = \varphi_{z=0} + 4\pi\sigma_g z / \epsilon_s$ takes place in the substrate region $d > z > 0$, where $\rho_z = 0$. In the gate region $z < 0$ Eq. (2) is transformed into the second-order differential equation

$$\frac{d^2\varphi_z}{dz^2} = \frac{4\pi|e|}{\epsilon} \begin{cases} n_A - n_{hz}, & (p\text{-Si}) \\ n_{ez} - n_D, & (n\text{-Si}) \end{cases}, \quad (4)$$

which is written for *p*-Si (*n*-Si) through the differences between acceptor (donor) and hole (electron) concentrations, n_A (n_D) and n_{hz} (n_{ez}). The boundary conditions

*Electronic address: ftvasko@yahoo.com

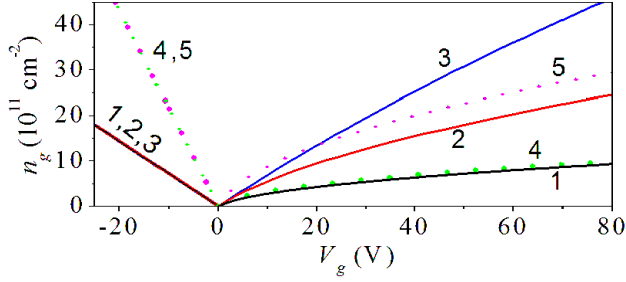


FIG. 2: Concentration of carriers n_g (electrons if $V_g > 0$ or holes if $V_g < 0$) versus gate voltage V_g for graphene on SiO_2 substrate of 300 nm or 100 nm width (solid or dotted curves) placed over p -Si gate with doping levels: $n_A = 10^{15} \text{ cm}^{-3}$ (1,4), 10^{16} cm^{-3} (2,5), and 10^{17} cm^{-3} (3).

for Eq. (4) are $\varphi_{z \rightarrow -\infty} = 0$ and the right Eq. (3), which determines an electric field at $z \rightarrow -0$.

Below, we restrict ourselves by the case of p -doped Si, where the non-degenerate hole approximation $n_{hz} = n_A \exp(e\varphi_z/T)$ is valid for $n_A \leq 5 \times 10^{18} \text{ cm}^{-3}$ at room temperature $T = 300 \text{ K}$. For higher n_A or for the n -doping case, n_{hz} or n_{ez} depend weakly on φ_z and deviations from Eq. (1) are weak. Since Eq. (4) does not depend on z explicitly, we obtain the first-order nonlinear equation

$$\left(\frac{e}{T} \frac{d\varphi_z}{dz} \right)^2 = \frac{2}{z_T^2} \left(e^{e\varphi_z/T} - \frac{e\varphi_z}{T} - 1 \right), \quad (5)$$

where the characteristic length z_T is determined by the relation $(4\pi e^2/\epsilon T)n_A z_T^2 = 1$. Further integration gives the potential and charge distributions, which are schematically shown in Figs. 1b and 1c, and $\varphi_{z=0}$ is connected with n_g through the boundary condition at $z \rightarrow -0$:

$$e^{v_0} - v_0 - 1 = \frac{1}{2} \left(\frac{n_g}{n_T} \right)^2, \quad v_0 \equiv \frac{e\varphi_{z=0}}{T}. \quad (6)$$

Here we introduce the characteristic 2D concentration $n_T = n_A z_T \propto \sqrt{n_A T}$ which is about $0.8 \times 10^{10} \text{ cm}^{-2}$ if $n_A = 10^{15} \text{ cm}^{-3}$ and $T = 300 \text{ K}$. Neglecting the low-doped region $n_g \leq n_T$, we obtain the simple relation between V_g and n_g :

$$\alpha V_g \simeq \mp n_g + n_T \frac{\epsilon_s z_T}{\epsilon d} \begin{cases} (n_g/n_T)^2/2, & \text{(h)} \\ -2 \ln(n_g/\sqrt{2}n_T), & \text{(e)} \end{cases}, \quad (7)$$

which generalize the standard plane capacitor formula given by Eq. (1). For the electron-doping case ($V_g > 0$), both $\propto n_g$ and $\propto n_g^2$ contributions are essential depending on the dimensionless factor $\epsilon_s z_T/\epsilon d$. By contrast, for the hole-doping case ($V_g < 0$) the \ln -correction can be only detected in the low-doped graphene. Note, that there is no temperature dependency for $V_g < 0$ and these dependencies are weak (appears in \ln -correction) for $V_g > 0$.

Fig.2 shows the carriers concentrations versus V_g in graphene placed over the SiO_2/p -Si structure depending on doping level and substrate thickness, n_A and d .

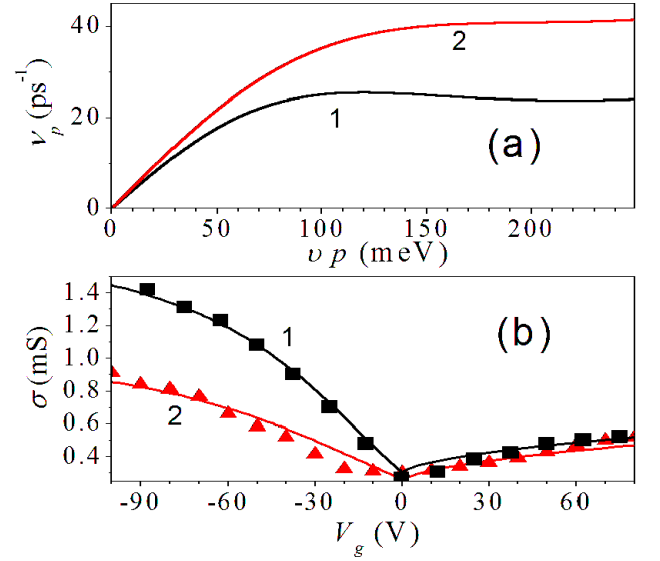


FIG. 3: (a) Fitting of experimental data from Refs. 4 and 5 marked as 1 and 2: (a) momentum relaxation rate ν_p versus energy vp and (b) conductivity σ versus V_g . Squares and triangles are experimental points from Refs. 4 and 5, respectively.

These dependencies are substantially different for e - and h -doping regimes. If $V_g < 0$, the plane capacitor approximation (1), with the n_A -independent concentration $n_g \propto d^{-1}$, is valid. If $V_g > 0$, the dependency $n_g(V_g)$ varies from the square-root to linear function and the electron-hole symmetry is restored if n_A exceeds 10^{17} cm^{-3} at $d = 300 \text{ nm}$. For thinner substrates ($d = 100 \text{ nm}$ is shown), the symmetry is restored at higher concentrations. The square-root dependency for low-doped p -Si appears due to the depleted region of thickness d_{depl} (see Fig. 1b), which is determined by the charge neutrality condition, $n_s \simeq n_A d_{\text{depl}}$. Using Eq. (1) with $d \rightarrow d + d_{\text{depl}}$, one obtains $n_s \propto \sqrt{V_g}$ for the case $d_{\text{depl}} \gg d$.

The asymmetrical electrostatic doping of graphene under sign-flip of V_g leads to similar changes of the gate voltage dependencies of static conductivity, $\sigma(V_g)$. These dependencies in structures placed on p -Si with $n_A \simeq 10^{15} \text{ cm}^{-3}$ were measured [4, 5] under investigations of the Drude and interband absorption in large-area samples. In order to fit $\sigma(V_g)$ we use the phenomenological momentum relaxation rates ν_p suggested in Ref. 7 with the parameters taken from the experimental data of Refs. 4 and 5 for the hole doping cases $V_g < 0$, when Eq. (1) is valid, see Fig. 2. Using the relaxation rates shown in Fig. 3a and the dependencies $n(V_g)$ for $V_g > 0$, we obtain an excellent agreement between $\sigma(V_g)$ and the results of Refs. 4 and 5, as it is shown in Fig. 3b. The asymmetry of $\sigma(V_g)$ is more pronounced than $n(V_g)$ (c.f. Figs. 2 and 3b) because of an additional energy dependency of ν_p .

Further, we turn to consideration of the structure with a thin high- κ substrates placed over p -Si. For these structures, Eq. (7) contains the parameter $\epsilon_s z_T/\epsilon d \gg 1$ and a

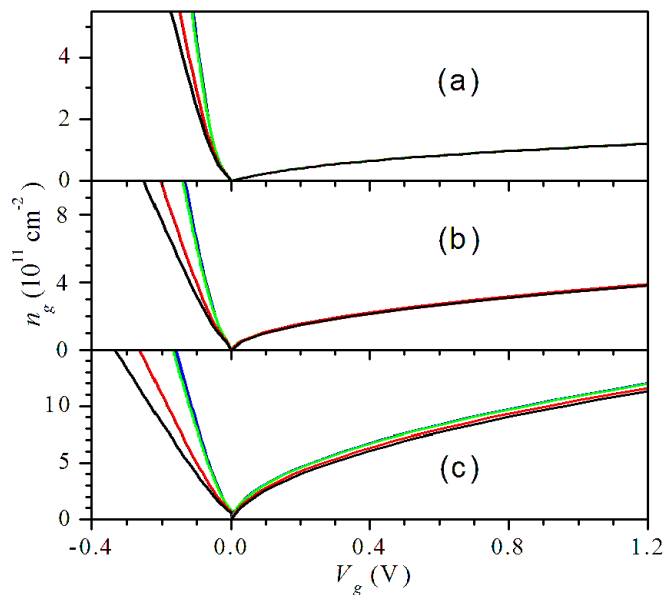


FIG. 4: (a) Concentration n_g versus V_g for graphene on AlN (black), Al_2O_3 (red), HfO_2 (green), and ZrO_2 (blue) substrates of width 10 nm placed over p -Si of doping level 10^{15} cm^{-3} . (b) and (c) The same for p -Si of doping levels 10^{16} cm^{-3} and 10^{17} cm^{-3} , respectively.

deviation from the standard formula (1) increases. Similar to Fig. 2, the dependencies of concentrations n_s on V_g are shown in Fig. 4 for AlN, Al_2O_3 , HfO_2 , and ZrO_2 substrates [8] of width 10 nm at different doping levels. Here the square-root behavior of $n(V_g)$, which is weakly dependent on ϵ_s , takes place at $V_g > 0$. For the hole doping regime, concentrations $n(V_g)$ deviate from the linear functions at low $|V_g|$, due to the \ln -contributions in Eq. (7), and curves are different for different substrates due to variations of ϵ_s . For higher doping levels n_A , the induced concentration n_g increases with V_g faster, c.f. Figs. 4a-4c where n_A varies from 10^{15} to 10^{17} cm^{-3} . The interval of V_g applied is restricted by the breakdown condition $V_g/d < 5 - 10 \text{ MV/cm}$, [9] so that we consider the region $|V_g| \leq 5 \text{ V}$.

The essential asymmetry of electron-hole doping changes conditions for interband absorption because of a different Pauli blocking effect for $V_g > 0$ and < 0 . At low temperatures (or for heavily-doped graphene) the absorption is blocked in the spectral region $\hbar\omega \leq 2\epsilon_F$. Here the Fermi energies of electrons and holes $\epsilon_F \propto \sqrt{n_g}$ depend on V_g asymmetrically, see Figs. 2 and 4. So that, the threshold of absorption spectra for $V_g > 0$ and < 0 should be different: at fixed $\hbar\omega$, higher threshold bias is necessary for the electron doping regime, i.e. the asymmetric Pauli blocking takes place. In Fig. 5a we plot the electron and hole Fermi energies versus the gate voltage for structures with Al_2O_3 substrate of different widths placed over p -Si of different doping levels. Similarly to Fig. 4, there is a visible dependency on n_A if $V_g > 0$ while for $V_g < 0$ the dependency of ϵ_F on d is only essential. The dependencies $\epsilon_F(V_g)$ for structures with the all

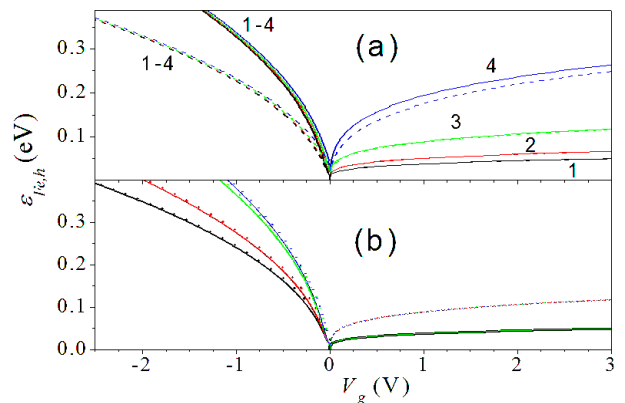


FIG. 5: Electron and hole Fermi energies versus gate voltage V_g for Al_2O_3 substrate of widths $d = 7$ and 15 nm (solid and dashed curves) at p -Si doping levels 10^{15} , 10^{16} , 10^{17} , 10^{18} cm^{-3} marked 1 to 4, respectively. (b) The same for different substrates [AlN (black), Al_2O_3 (red), HfO_2 (green), and ZrO_2 (blue)] of widths $d = 10 \text{ nm}$ at p -Si doping levels 10^{15} and 10^{17} cm^{-3} (solid and dashed curves, respectively).

high- κ substrates under consideration are shown in Fig. 5b for low- and heavily doped p -Si. Once again, $\epsilon_F(V_g)$ is not dependent on ϵ_s at $V_g > 0$ and the dependencies on n_A are negligible at $V_g < 0$. Note, that the threshold of absorption appears at low voltages for the hole doping case, $V_g \geq -1 \text{ V}$ if $\hbar\omega \leq 0.6 \text{ eV}$. For the electron doping case, there is no threshold up to the breakdown voltage, if $\hbar\omega \geq 0.3 \text{ eV}$.

An essential distinction between the spectral dependencies of interband absorption for the electron and hole doping regimes was reported in Refs. 4 and 5 for the structures of large-area graphene placed on SiO_2 substrate over low-doped p -i. These results are in a qualitative agreement with the asymmetrical dependencies of $\epsilon_F(V_g)$ which can be obtained from Fig. 2. But a quantitative description of the dynamic conductivity σ_ω should take into account both the temperature broadening and the disorder effects, similar the consideration of the hole doping regimes performed recently, [10] and it requires a special consideration. Here we consider the asymmetrical threshold of interband absorption in the graphene-based modulator with the Al_2O_3 substrate of width 7 nm and the waveguide designed for the telecommunication spectral range, $\hbar\omega \simeq 0.8 \text{ eV}$. [6] The depth of modulation, ΔT_ω , should be proportional to the carrier-induced contribution of the dynamic conductivity, $\Delta T_\omega \propto \text{Re}\Delta\sigma_\omega$, where $\text{Re}\Delta\sigma_\omega$ is given by [10]

$$\text{Re}\Delta\sigma_\omega = \frac{\sigma_{\text{inter}}}{\exp[(\hbar\omega - 2\epsilon_F)/2T] + 1}, \quad \sigma_{\text{inter}} = \frac{e^2}{4\hbar}. \quad (8)$$

Here we consider the case $\epsilon_F \gg T$, so that the chemical potential is replaced by ϵ_F . Using $\epsilon_F(V_g)$ shown in Fig. 5, below we consider the dependency of $\Delta T_\omega \propto \text{Re}\Delta\sigma_\omega$ on V_g normalized to the unit amplitude of modulation.

The normalized conductivity $2\text{Re}\sigma_\omega/\sigma_{\text{inter}}$ is plotted in Fig. 6 for the conditions of Ref. 6 at different doping

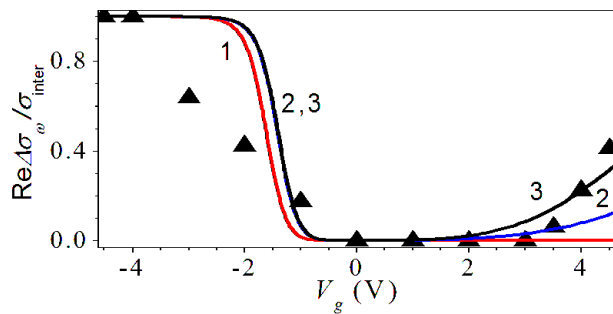


FIG. 6: Dissipative interband conductivity $\text{Re}\Delta\sigma_\omega$, normalized to σ_{inter} , versus V_g for graphene on Al_2O_3 substrate at p -Si doping levels 10^{15} (1), 2×10^{18} (2), and $3 \times 10^{18} \text{ cm}^{-3}$ (3). Triangles show experimental data for ΔT_ω from Ref. 6 which are normalized to the amplitude of modulation.

levels of p -Si. One can see, that the experimental data for the normalized dependency of ΔT_ω on V_g can be fitted at $n_A \simeq 3 \times 10^{18} \text{ cm}^{-3}$ and $T = 300 \text{ K}$ (a doping level is not given in [6] and we use n_A as a single fitting parameter). The thresholds of absorption are in good agreement with the measurements both for the electron and hole doping regimes but the temperature-induced smearing leads to more abrupt jumps in comparison to the experimental spectra. It is because a disorder contribution did not taken into account, see similar analysis of the interband absorption spectra [4, 5] in Ref. 10. In addition, the narrow waveguide structure forms a strip-like capacitor with the non-uniform charge distribution across the waveguide; [11] this leads to an additional smearing effect. There is a weak doping dependency of ΔT_ω at

$V_g < 0$ and at $V_g > 0$ the modulation condition $\hbar\omega \sim 2\varepsilon_F$ satisfies if $n_A \geq 10^{18} \text{ cm}^{-3}$. The last estimate is valid for the in-plane homogeneous structure, while for a bus waveguide [6] doping level should be lower. A complete description of the results of Ref. 6 requires to take into account both the disorder contributions and the waveguide geometry.

Now we list the assumptions used in our calculations. The consideration of the non-degenerate holes is valid for any n_A and any V_g because of formation of the depletion region at $V_g > 0$ and weak corrections to Eq. (1) at $V_g < 0$. Apart from the mechanism under consideration, the Coulomb renormalization in n - or p -doped graphene leads to an additional (up to 10%) asymmetry of response. [3, 12] Such a contribution can be neglected in the structures analyzed here (with a low-doped p -Si gate or a thin high- κ substrate). But in typical samples (with the electron-hole asymmetry $\leq 10\%$) both the Coulomb effect and the electrostatic contribution should be taken into account. This could result in decrease or increase of the electron-hole asymmetry. In the vicinity of the zero bias, $V_g \approx 0$, the long-range disorder [13] should modify the effect under consideration.

Summarizing, the mechanism of the electron-hole symmetry breakdown, caused by different drops of potentials in low-doped Si for opposite signs of bias, have been analyzed and the results are in agreement with the recent transport and optical measurements. These results are also important for device applications such as the field effect transistors [14] or the high-frequency multipliers. [15]

-
- [1] A. H. Castro Neto, F. Guinea, N. M. R. Peres, K. S. Novoselov, and A. K. Geim, *Rev. Mod. Phys.* **81**, 109 (2009); N. M. R. Peres, *Rev. Mod. Phys.* **82**, 2673 (2010); S. Das Sarma, S. Adam, E. H. Hwang, and E. Rossi, *Rev. Mod. Phys.* **83**, 407 (2011).
- [2] L. A. Falkovsky, *Phys. Usp.* **51**, 887 (2008); M. Orlita and M. Potemski, *Semicond. Sci. Technol.* **25**, 063001 (2010); F. Bonaccorso, Z. Sun, T. Hasan, and A. C. Ferrari, *Nature Photonics* **4**, 611 (2010); K. F. Mak, L. Ju, F. Wang, and T. F. Heinz, *Solid State Commun.* **152**, 1341 (2012).
- [3] V. N. Kotov, B. Uchoa, V. M. Pereira, F. Guinea, and A. H. Castro Neto, *Rev. Mod. Phys.* **84**, 1067 (2012).
- [4] J. Horng, C.-F. Chen, B. Geng, C. Girit, Y. Zhang, Z. Hao, H. A. Bechtel, M. Martin, A. Zettl, M. F. Crommie, Y. R. Shen, and F. Wang, *Phys. Rev. B* **83**, 165113 (2011).
- [5] L. Ren, Q. Zhang, J. Yao, Z. Sun, R. Kaneko, Z. Yan, S. Nanot, Z. Jin, I. Kawayama, M. Tonouchi, J. M. Tour, and J. Kono, *Nano Lett.* **12**, 3711 (2012).
- [6] M. Liu, X. Yin, E. Ulin-Avila, B. Geng, T. Zentgraf, L. Ju, F. Wang, and X. Zhang, *Nature* **474**, 64 (2011).
- [7] P. N. Romanets and F. T. Vasko, *Phys. Rev. B* **83**, 205427 (2011); F. T. Vasko and V. Ryzhii, *ibid.* **76**, 233404 (2007).
- [8] We used the static dielectric permittivities $\epsilon_s \simeq 9.4, 12.5, 22$, and 24 , for AlN , Al_2O_3 , HfO_2 , and ZrO_2 , respectively. These data are given by M. V. Fischetti, D. A. Neumayer, and E. A. Cartier, *J. Appl. Phys.* **90**, 4587 (2001).
- [9] H. Wang, Y. Wu, C. Cong, J. Shang, and T. Yu, *ACS Nano* **4**, 7221 (2010); P. D. Ye, G. D. Wilk, B. Yang, J. Kwo, H. J. L. Gossman, M. Hong, K. K. Ng, and J. Bude, *Appl. Phys. Lett.* **4** (2004) 434.
- [10] F. T. Vasko, V. V. Mitin, V. Ryzhii, and T. Otsuji, *Phys. Rev. B* **86**, 235424 (2012).
- [11] F. T. Vasko and I. V. Zozoulenko, *Appl. Phys. Lett.* **97**, 092115 (2010).
- [12] A. G. Grushin, B. Valenzuela, and M. A. H. Vozmediano, *Phys. Rev. B* **80**, 155417 (2009); N. M. R. Peres, R. M. Ribeiro, and A. H. Castro Neto, *Phys. Rev. Lett.* **105**, 055501 (2010); S. H. Abedinpour, G. Vignale, A. Principi, M. Polini, W.-K. Tse, and A. H. MacDonald, *Phys. Rev. B* **84**, 045429 (2011).
- [13] J. Martin, N. Akerman, G. Ulbricht, T. Lohmann, J. H. Smet, K. von Klitzing, and A. Yacoby, *Nat. Phys.* **4**, 144 (2007); Y. Zhang, V.W. Brar, C. Girit, A. Zettl, and M. F. Crommie, *ibid.* **6**, 722 (2009).
- [14] F. Schwierz, *Nature Nanotech.* **5**, 487 (2010); D. Reddy,

- L. F. Register, G. D. Carpenter, and S. K. Banerjee, *J. of Phys. D* **44**, 313001 (2011).
- [15] H. Wang, A. Hsu, J. Wu, J. Kong, and T. Palacios, *IEEE Electr. Dev. Lett.*, **31**, 906 (2010).